2026 IEEE/SICE International Symposium on System Integration (SII)
January 11-14, 2026. Cancún, México

Object Deformation Suppression for Grasping Leveraging Optical Proximity Sensors

Shunsuke Tokiwa, Hikaru Arita, Yosuke Suzuki, Kazuto Nakashima, and Kenji Tahara

Abstract— **Grasping soft and individualized food and agricultural products without causing damage is a significant challenge in robotics. This task requires balancing two conflicting demands: applying sufficient force to lift the object and avoiding excessive force that could cause damage. Conventional approaches include learning-based manipulation and sequential control based on slip detection. However, the former requires prior training, while the latter takes time to adjust the grasping force. Therefore, these methods are not suitable for environments where object properties change frequently or for high-throughput operations. To address these issues, we propose a parameter adaptation method for deformation suppression that does not require learning and enables high-speed processing. The proposed method reduces the grasping force according to object deformation, which is detected by optical proximity sensors. A key benefit of optical proximity sensors is high-speed data acquisition, which enables real-time adjustment of grasping force without stopping the motion, leading to faster task completion. Furthermore, the deformation information obtained from the proximity sensor is converted into a virtual force, and the grasping force is adjusted based on the virtual dynamics framework. This enables seamless integration with pre-grasp control strategies that gently approach the object.**

I. INTRODUCTION

Many grippers used in factory settings primarily target known objects with pre-defined shapes and stiffness, achieving highly efficient grasping through repetitive motions. On the other hand, many processes where automation has not progressed involve objects whose geometric and mechanical properties are not unique, making them challenging for conventional robots that excel at repetitive tasks. For instance, grasping soft objects with individual differences, such as food products and agricultural produce, remains one of the critical challenges in robotics [1][2]. These objects vary in shape and stiffness from one individual to another and are often fragile and easily damaged, making it difficult to apply grasping strategies that assume known objects. In general, grasping tasks require simultaneously satisfying the following contradictory requirements, and this balance becomes particularly critical when dealing with soft and fragile objects:

- Exerting sufficient grasping force to achieve tasks such as lifting the object.
- Avoiding excessive force that could damage the object.

*This work was partially supported by JSPS KAKENHI Grant Number JP24H00726 .

S. Tokiwa, H. Arita, K. Nakashima and K. Tahara are with Department of Mechanical Engineering, Kyushu University, Fukuoka 819-0395, Japan (e-mail: tokiwa@hcr.mech.kyushu-u.ac.jp; [arita, kazuto, tahara]@ieee.org).

Yosuke Suzuki is with the Faculty of Frontier Engineering, Institute of Science and Engineering, Kanazawa University, Kanazawa, Ishikawa 920-1192, Japan (e-mail: suzuki@se.kanazawa-u.ac.jp).

To address these conflicting demands, control utilizing vision-based tactile sensors has proven effective. In recent years, research has advanced using high-resolution and low-cost sensors such as GelSight and DIGIT [3][4][5][6]. Approaches that leverage these sensors can be broadly categorized into two types: learning-based methods [3][4] and non-learning-based slip detection control [5]. While the former can achieve a high grasping success rate for diverse object types through learning, it incurs time and cost due to the need for data collection and retraining whenever the object or sensor changes [3][4]. The latter can function independently of object properties through sequential adjustments, but faces the challenge of longer processing times per item, making it unsuitable for high-speed operations [5]. When there is a large variation in the weight of the target objects, this issue becomes particularly pronounced. This is because the control is designed to exert only the minimum necessary force to prevent the object from being dropped, rather than adjusting the force in response to object deformation.

To address these challenges, we propose a parameter adaptation method that does not require learning, enables high-speed processing, and can handle objects with unknown mechanical and geometric properties. The proposed method is characterized by the following two key features:

- High-speed sensing of object deformation using optical proximity sensors
- Adaptive adjustment of control parameters that govern the grasping force

Particularly, this study focuses on one of the aforementioned requirements: Avoiding excessive force that could damage the object. Although optical proximity sensors have been widely employed for pre-grasp sensing [7][8][9], their utilization in the post-grasp phase has rarely been explored. The method utilizes a hybrid proximity sensor combining the reflectance light intensity type (O-RLI-type) and the time-of-flight type (O-ToF-type) . The O-RLI-type acquires proximity information based on the intensity of reflected light from an object [10], and it exhibits a characteristic where the output increases as the contact area between the fingertip and the object expands. This means that the output increases as the object deforms to “conform” to the finger, thereby enabling the detection of object deformation. Such deformation is commonly observed in various agricultural products and food, including strawberries, grapes, and walleye pollack roe. However, the O-RLI-type output increases not only due to deformation but also due to approach, necessitating a distinction between increases caused by approach and those

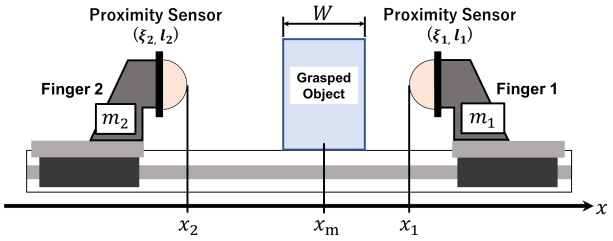

Fig. 1. The control target in this study is a two-finger parallel gripper. Optical proximity sensors (O-RLI-type and O-ToF-type) are attached to the tips of each finger.

caused by deformation. To resolve this, by concurrently using the O-ToF-type, which detects the distance to the object, output increases due to approach are distinguished from those due to deformation. Although vision-based tactile sensors can also detect deformations that conform to the fingertip, their response speed can be a limiting factor. In general, vision-based tactile sensors have a sampling rate of around 10 to 90 Hz [11][12][13], whereas O-RLI-type proximity sensors can sample at approximately 1 kHz. Therefore, in situations where an object deforms rapidly, even if a control algorithm similar to the method proposed later in this paper is used with a tactile sensor, it may not be able to reduce the grasping force in time. Thus, not only the concept of control based on slip detection but also the characteristics of the sensor itself can be unsuitable for high-speed processing.

In this study, we propose an adaptive adjustment strategy for control parameters that govern the grasping force. The parameter adjustment is based on the rate of change in the output of the proximity sensor, as utilized in [7][14]. According to the model of the O-RLI-type sensor, this rate of change reflects the deformation characteristics at the contact interface. Furthermore, the deformation information is converted into a virtual force, and a control framework called MVDC (Multiple Virtual Dynamics-based Control) [7][14] is employed. We introduce a novel idea of extending MVDC not as a trajectory planner for robot coordinates, as in [7][14], but as a planner for control parameters that govern the grasping force. By implementing deformation suppression within the MVDC framework, it becomes possible to integrate with pre-contact control (simultaneous contact and impact reduction control) [7], thereby achieving consistent and delicate grasping control across both pre-contact and post-contact phases without switching control laws.

This work introduces a fast, learning-free control method using optical proximity sensing to interact safely with fragile, variable objects. Focusing on suppressing deformation during contact, the method forms a basis for robust and adaptable robotic grasping.

II. Overview of the Control Target and Proximity Sensors

As the simplest example, a two-finger parallel gripper is used as the control target in this study, as shown in Fig. 1. A hybrid optical proximity sensor, equipped with both O-RLI-type and O-ToF-type components, is attached to the fingertip of each finger. The information on the grasped object is obtained from these sensors. Each finger of the gripper can be treated as an independent 1-degree-of-freedom (DoF) system. Considering that the x coordinate is attached to the gripper wrist, the motion of each finger is modeled as follows:

$$m_j \ddot{x}_j = u_j + f_{\mathrm{c}j}, \tag{1}$$

where m_j is the mass of the gripper finger, x_j is the fingertip position, u_j is the control input, $f_{\mathrm{c}j}$ is the contact force acting from the grasped object, and subscripts $j = 1$ and 2 indicate the right and left fingers of the gripper, respectively.

III. Method

Fig. 2 shows the block diagram of the proposed controller, in which parameter adaptation for deformation suppression is newly added to the simultaneous contact, impact reduction, and contact force control proposed in [7]. The parameter adaptation for deformation suppression is incorporated into the first layer, which plays the role of contact force control, and consists of Virtual force generator A and Virtual dynamics A.

A. Simultaneous contact, impact reduction, and force control

Each finger of the gripper is controlled by MVDC, which consists of three layers. The third layer plays the role of simultaneous contact control. The virtual dynamics 2 is given by

$$M_{\mathrm{a},2}(\ddot{x}_{\mathrm{v},2} - \ddot{x}_{\mathrm{d}}) + D_{\mathrm{a},2}(\dot{x}_{\mathrm{v},2} - \dot{x}_{\mathrm{d}}) + K_{\mathrm{a},2}(x_{\mathrm{v},2} - x_{\mathrm{d}}) = f_{\mathrm{s}}, \tag{2}$$

where $M_{\mathrm{a},k}$, $D_{\mathrm{a},k}$, and $K_{\mathrm{a},k}$ are the mass, viscosity coefficient, and elastic coefficient of the virtual object k ($k = 1, 2$), and $x_{\mathrm{v},2}$, $\dot{x}_{\mathrm{v},2}$, and $\ddot{x}_{\mathrm{v},2}$ are the position, velocity, and acceleration of the virtual object 2 determined by virtual dynamics 2. Here, the virtual object is a non-existent object considered to reflect the effect of virtual force on motion of control target. Additionally, x_{d}, $\dot{x}_{\mathrm{d}}$, and $\ddot{x}_{\mathrm{d}}$ are the target trajectories, which are given by the trajectory planner as follows:

$$x_{\mathrm{d}} = \frac{x_1 + x_2}{2}, \ \dot{x}_{\mathrm{d}} = 0, \ \ddot{x}_{\mathrm{d}} = 0. \tag{3}$$

The virtual force f_{s} calculated by virtual force generator 2 is given by $f_{\mathrm{s}} = K_{\mathrm{s}} \tanh((\xi_1 - \xi_2)/(\xi_1 + \xi_2))$, where ξ_j is the output of the O-RLI-type proximity sensor and K_{s} is the gain.

The second layer plays the role of impact reduction. The virtual dynamics 1 is given by

$$\begin{aligned} M_{\mathrm{a},1}(\ddot{x}_{\mathrm{v}j,1} - \ddot{x}_{\mathrm{v},2}) + D_{\mathrm{a},1}(\dot{x}_{\mathrm{v}j,1} - \dot{x}_{\mathrm{v},2}) \\ + K_{\mathrm{a},1}(x_{\mathrm{v}j,1} - x_{\mathrm{v},2}) = f_{\mathrm{p}j}, \end{aligned} \tag{4}$$

where $x_{\mathrm{v}j,1}$, $\dot{x}_{\mathrm{v}j,1}$, and $\ddot{x}_{\mathrm{v}j,1}$ are the position, velocity, and acceleration of the virtual object 1 determined by virtual dynamics 1. The virtual viscous force $f_{\mathrm{p}j}$ calculated by virtual force generator 1 is given by $f_{\mathrm{p}j} = D_{\mathrm{p}j}\dot{\xi}_j/\xi_j$, where $D_{\mathrm{p}j}$ is the viscosity coefficient.

The first layer is an impedance control that plays the role of contact force control. The first layer uses the position $x_{\mathrm{v}j,1}$ and velocity $\dot{x}_{\mathrm{v}j,1}$ of the virtual object 1 obtained in

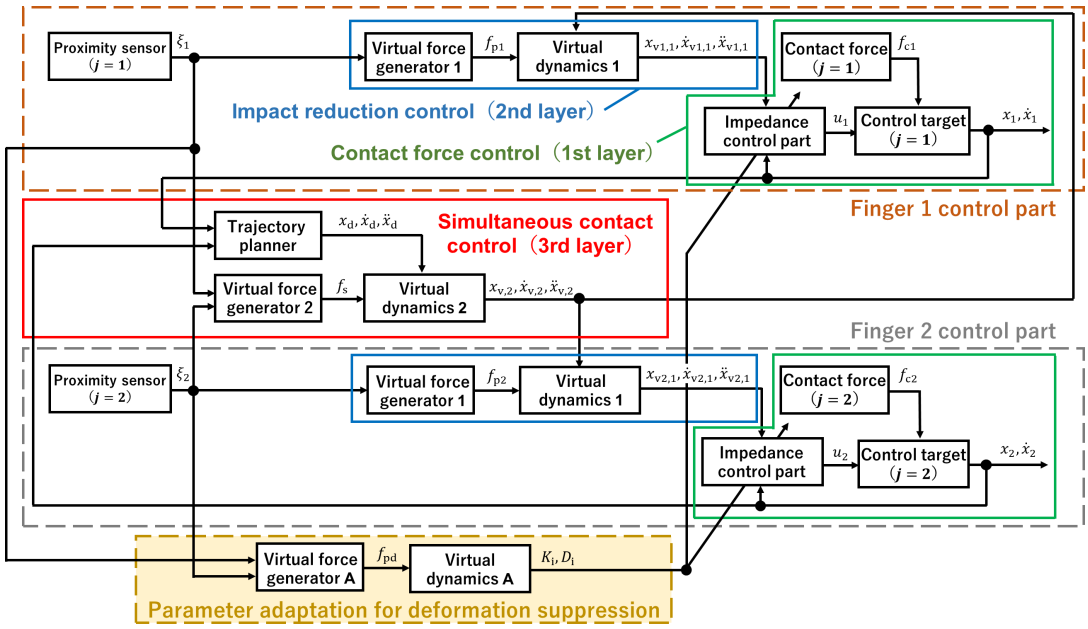

Fig. 2. Block diagram of the proposed controller using MVDC. A virtual dynamics is newly introduced to the control parameters of impedance control, allowing the contact force control to attenuate the grasping force in accordance with object deformation.

the second layer as the desired state. Since no force sensor is mounted on the fingers in this research, no inertia-related control is performed, and m_j is left as is. In this case, u_j is given as follows:

$$u_j = -D_{\mathrm{i}}(\dot{x}_j - \dot{x}_{\mathrm{v}j,1}) - K_{\mathrm{i}}(x_j - x_{\mathrm{v}j,1}), \tag{5}$$

where D_{i} and K_{i} are the desired viscosity and elastic coefficients in impedance control.

B. Parameter adaptation for deformation suppression

The parameter adaptation proposed in this study introduces virtual dynamics into the impedance control parameters K_{i} and D_{i} in (5). The virtual force f_{pd} calculated by virtual force generator A is given by

$$f_{\mathrm{pd}} = \begin{cases} 0 & (l_1 + l_2 > \epsilon) \\ -D_{\mathrm{pd}}\left(\frac{\dot{\xi}_1}{\xi_1} + \frac{\dot{\xi}_2}{\xi_2}\right) & (l_1 + l_2 \leq \epsilon) \end{cases}, \tag{6}$$

where D_{pd} is the gain, l_j is the distance between the proximity sensor and the object surface (output of O-ToF-type), and ϵ is a small number determined by the performance of O-ToF-type. Since the O-ToF-type generally does not have a detection distance of zero millimeters, ϵ is determined by the sum of the minimum detectable distances of the O-ToF-type on each finger, and contact is assumed when this threshold is reached. When contact is assumed, the virtual force f_{pd} is activated. Although f_{pd} becomes a discontinuous input at the moment of contact, it is used as an input to the virtual dynamics described later, so the behavior of K_{i} and D_{i} remains continuous and does not lead to unstable behavior.

Subsequently, by substituting the O-RLI-type sensor output model into (6), it is shown that (6) depends on the temporal change in a parameter related to the shape of the contact surface. The output of an O-RLI-type sensor is modeled as follows [8]:

$$\xi_j = G_\xi \frac{\alpha_j \psi}{(l_j + l_0)^{n_j}}, \tag{7}$$

where G_ξ is the coefficient for the transformation from the amount of light received to a voltage determined by a sensing element such as a phototransistor, ψ is the light energy emitted from the LED, l_0 is the offset distance to prevent direct contact between the sensor element and the object, α is the reflectance of the object surface, and n is the diffusion coefficient, which depends on the arrangement of LEDs and phototransistors, and the shape of the detected surface. In particular, focusing on the post-contact phase, $l_j = 0$, and under this condition, both sides of (7) are differentiated with respect to time t. Considering that the only time-dependent parameter is n, the following equation is obtained:

$$\dot{\xi}_j = G_\xi \frac{\alpha_j \psi}{{l_0}^{n}} \frac{\mathrm{d}n_j}{\mathrm{d}t} \log\left(\frac{1}{l_0}\right). \tag{8}$$

Therefore, $f_{\mathrm{pd}}\,(l_1 + l_2 \leq \epsilon)$ is expressed as follows:

$$f_{\mathrm{pd}} = -D_{\mathrm{pd}} \log\left(\frac{1}{l_0}\right)\left(\frac{\mathrm{d}n_1}{\mathrm{d}t} + \frac{\mathrm{d}n_2}{\mathrm{d}t}\right). \tag{9}$$

In other words, the rate of change in the output of O-RLI-type after contact represents the time derivative of n. The parameter n depends on the shape of the contact surface, and its value increases as the object conforms more closely to the shape covering the sensor surface. That is, an increase in n after contact indicates that the object is deforming to better fit the fingertip sensor surface, and its time derivative corresponds to the temporal change in the progression of that deformation. Therefore, f_{pd} represents a virtual force

obtained by converting the average rate of change in deformation progression at each fingertip. Moreover, as indicated by the absence of the reflectivity coefficient α in (9), the virtual force defined in (6) is independent of surface reflectivity. This confirms that the parameter adaptation for deformation suppression can function robustly regardless of the object's optical properties.

In virtual dynamics A, f_{pd} is used as an external force on the virtual object A, and the dynamics is given by the following equation of motion:

$$M_{\mathrm{a,A}}\ddot{K}_{\mathrm{i}} + D_{\mathrm{a,A}}\dot{K}_{\mathrm{i}} = f_{\mathrm{pd}}, \tag{10}$$

where $M_{\mathrm{a,A}}$ and $D_{\mathrm{a,A}}$ are the mass and viscosity coefficient of the virtual object A. Furthermore, D_{i} is calculated as follows:

$$D_{\mathrm{i}} = 2\zeta_{\mathrm{i}}\sqrt{m_j K_{\mathrm{i}}}, \tag{11}$$

where ζ_{i} is the damping ratio.

According to (5), the grasping force at static equilibrium is determined by the product of the object's half-width and K_{i}. Therefore, the initial value of K_{i} can be set based on the object's width and the desired grasping force at static equilibrium. To estimate the object width W, the O-ToF-type sensor is used prior to grasping, and W is calculated as $W = (x_1 - x_2) - (l_1 + l_2)$. Assuming that the desired grasping force at static equilibrium is F_{d}, the initial value of K_{i}, denoted as $K_{\mathrm{i,init}}$, is given by:

$$K_{\mathrm{i,init}} = \frac{2F_{\mathrm{d}}}{W}. \tag{12}$$

When the object does not deform, K_{i} remains constant at $K_{\mathrm{i,init}}$, and F_{d} is applied. On the other hand, when the object deforms, the grasping force decreases from F_{d} according to (10).

IV. Evaluation by Simulations

In this section, the proposed method is evaluated via simulations. Simulink in MATLAB is used as the simulation software.

A. Simulation Conditions

1) Modeling of the Grasped object: In this simulation, the grasped object is modeled as a massless elastic body, and various object stiffnesses are represented by varying the spring constant. In this case, the contact force $f_{\mathrm{c}j}$ exerted on the fingertip by the object is given by the following equation:

$$f_{\mathrm{c1}} = K\Delta W = K\{W - (x_1 - x_2)\},\ f_{\mathrm{c2}} = -K\Delta W, \tag{13}$$

where $\Delta W \geqq 0$ is the change in object width (Amount of finger sinkage into the object), and K is the stiffness of the object.

2) Modeling of the O-RLI-type Proximity Sensor Output: In this simulation, the output of O-RLI-type proximity sensor is modeled using the first-order exponential model [9] as shown in the following equation:

$$\xi_j = a\exp(cl_j), \tag{14}$$

where $a > 0$ and $c < 0$ are approximate parameters. However, in this simulation, it is necessary to treat the output change after contact, so the case where the finger sinks against the object is treated as $l_j < 0$, and its absolute value represents the depth of the sinking. Fig. 3 shows the relationship between the output ξ and l for the optical proximity sensor proposed in [15]. The contact surface used in the experiment is a white sponge (Gekiochi-kun, Lec Inc., Tokyo, Japan). The approximate parameters are $a = 1.4984$ and $c = -62.9326$, respectively, and the coefficient of determination is 0.9924. According to Fig. 3, fitted curve explains the experimental data well. Note that, if l_j falls outside the modeling range in the negative direction, (14) is no longer considered valid, and ξ_j is assumed to remain at the maximum output defined within the modeling range without further increase.

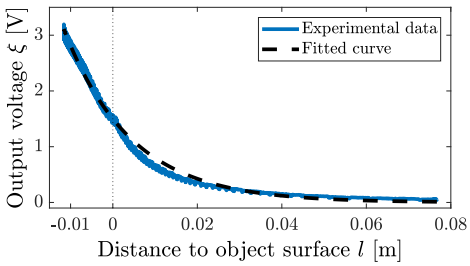

Fig. 3. Relationship between the sensor–object distance and proximity sensor (O-RLI-type) output when the contact surface is a white sponge. The blue curve represents the experimental data, and the dashed curve represents the fitted curve. $l < 0$ represents the amount of sinkage into the object.

TABLE I

Physical quantities related to the control target and the grasped object

$x_{\mathrm{init},1}$	$x_{\mathrm{init},2}$	m_j	W	x_{m}
0.11 m	−0.11 m	0.5 kg	0.06 m	0.03 m

B. Validation Cases

In this simulation, the following cases are verified to confirm the effectiveness of the proposed method.

Case 1:

A comparison is conducted between the case using the proposed method and the case in which the virtual force is set to zero (i.e., $D_{\mathrm{pd}} = 0$, meaning $K_{\mathrm{i}} = K_{\mathrm{i,init}}$ and $D_{\mathrm{i}} = 2\zeta_{\mathrm{i}}\sqrt{m_j K_{\mathrm{i,init}}}$). The time series data of K_{i}, contact force $|f_{\mathrm{c}j}|$, and fingertip position x_j are compared. In this evaluation, the object stiffness is set to $K = 100$ N/m.

Case 2:

The behavior of the steady-state values of K_{i}, contact force $|f_{\mathrm{c}j}|$, and depth of sinkage ΔW is evaluated under varying object stiffness K. In this evaluation, the stiffness of the object is varied from 50 N/m to 1000 N/m in increments of 2 N/m.

All simulations above are conducted under the physical and control parameters listed in Tables I and II.

TABLE II

CONTROL PARAMETERS

Simultaneous Contact Control				
	$M_{a,2}$	$D_{a,2}$	$K_{a,2}$	K_s
	1 kg	12 N·s/m	36 N/m	3 N
Impact Reduction Control				
	$M_{a,1}$	$D_{a,1}$	$K_{a,1}$	$D_{p1,2}$
	1 kg	10 N·s/m	25 N/m	±0.3 N·s
Parameter Adaptation for Deformation Suppression				
$M_{a,A}$	$D_{a,A}$	F_d	ζ_i	ϵ
1 kg	10 N·s/m	5 N	1	0.005 m

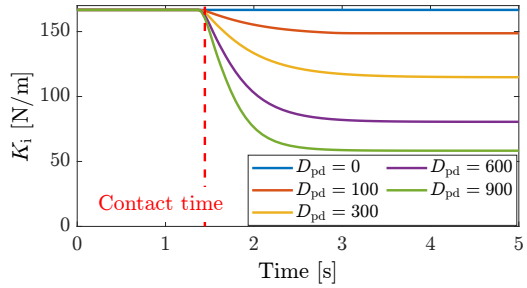

Fig. 4. Time series data of the control parameter K_i with different D_{pd} values (0 to 900 N·s). Each line represents a different D_{pd} setting applied during the grasping control.

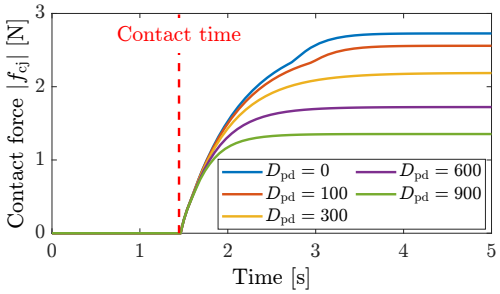

Fig. 5. Time series data of the contact force with different D_{pd} values (0 to 900 N·s). Each line represents a different D_{pd} setting applied during the grasping control.

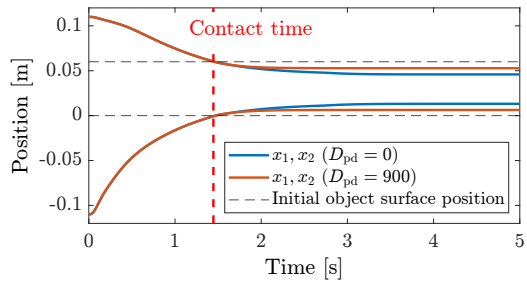

Fig. 6. Time series data of the fingertip position with $D_{pd} = 0$ and 900 N·s. The solid lines represent the coordinates of each finger, and the black dashed lines represent the initial coordinates of the object surface.

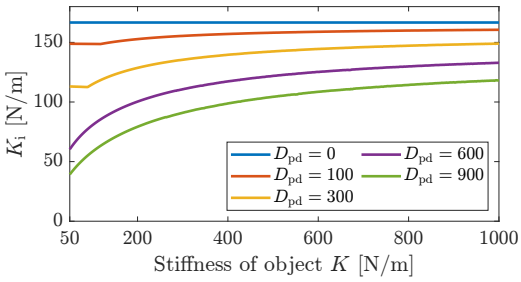

Fig. 7. Steady-state values of the control parameter K_i plotted against object stiffness K. Multiple lines correspond to different D_{pd} values from 0 to 900 N·s.

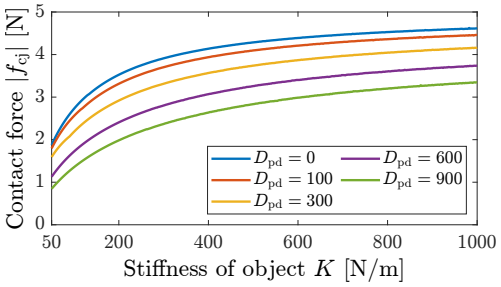

Fig. 8. Steady-state values of the contact force plotted against object stiffness K. Multiple lines correspond to different D_{pd} values from 0 to 900 N·s.

C. Simulation Results

1) Case 1: Time series data of K_i, the contact force, and the fingertip position for varying D_{pd} in the range of 0 to 900 N·s are shown in Fig. 4, Fig. 5, and Fig. 6, respectively. From Fig. 4 and Fig. 5, it can be observed that both K_i and the contact force decrease as D_{pd} increases. This indicates that D_{pd} is a parameter that determines the degree to which the grasping force is reduced in response to deformation; larger values of D_{pd} result in lower grasping forces. In particular, focusing on the case of $D_{pd} = 900$, K_i decreases from 166.7 N/m to 58.3 N/m, and the contact force decreases from 2.73 N to 1.35 N. Furthermore, comparing the depth of sinkage between the cases of $D_{pd} = 0$ and $D_{pd} = 900$ based on Fig. 6, the value is reduced from 27.3 mm (45.5 % against the initial width) to 13.5 mm (22.6 % against the initial width).

2) Case 2: The steady-state values of K_i, contact force, and depth of sinkage when the object stiffness K is varied in the range of 50 to 1000 N/m are shown in Fig. 7, Fig. 8, and Fig. 9, respectively. From Fig. 7, it can be observed that the reduction in K_i becomes larger as the object stiffness K decreases. Additionally, Fig. 8 shows that the amount of decrease in the contact force remains nearly constant regardless of the stiffness of the object. However, it should be noted that reducing the grasping force by 1 N for an object with $K = 50$ and doing the same for an object with $K = 1000$ have different effects in terms of reducing object deformation. As shown in Fig. 9, the reduction in the depth of sinkage becomes greater as K decreases. Specifically, for $D_{pd} = 900$, the reduction in sinkage is 0.021 m for $K = 50$

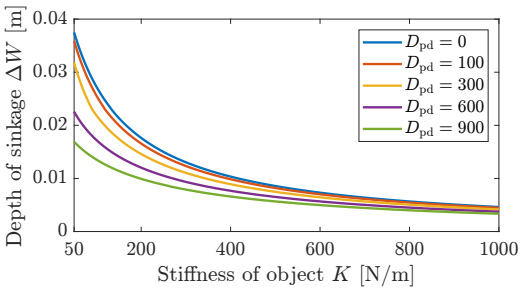

Fig. 9. Steady-state values of the fingertip sinkage into the object plotted against object stiffness K. Multiple lines correspond to different $D_{\rm pd}$ values from 0 to 900 N·s.

and 0.0013 m for $K = 1000$, indicating that the reduction for $K = 50$ is approximately 16.2 times greater than that for $K = 1000$. These results demonstrate that the softer the object, the greater the effect of reducing deformation.

3) Summary and Interpretation of Results: In the proposed method, the control parameters $K_{\rm i}$ and $D_{\rm i}$ are autonomously adjusted based on object deformation. This adjustment begins when the virtual force $f_{\rm pd}$, triggered by the output of the O-ToF-type sensor, becomes active. According to Fig. 4, $f_{\rm pd}$ becomes active 1.37 s after the start of grasping, and from that point, $K_{\rm i}$ is observed to decrease. Since the virtual force $f_{\rm pd}$ depends on the rate of change in the output of the O-RLI-type sensor, it becomes zero when the reaction force from the object and the exerted force from the fingertip are balanced (i.e., when the finger stops moving), and its influence disappears. At that point, the grasping force is determined based on $K_{\rm i}$ and $D_{\rm i}$ according to (5). In this way, because parameter adjustment is completed during the impedance control-based grasping process, the time required for the contact force to converge does not vary notably depending on whether the adjustment is performed or not. This can be confirmed from Fig. 5.

The extent of grasping force reduction is influenced by two main factors. One is the virtual force gain $D_{\rm pd}$. Increasing this value results in a larger $f_{\rm pd}$, leading to a greater decrease in $K_{\rm i}$ and thus stronger force attenuation. This allows the user to manually adjust the degree of deformation suppression. The other factor is the stiffness of the object. For softer objects, the indentation velocity at contact tends to be higher, which increases the rate of change in the O-RLI-type sensor output. As a result, $f_{\rm pd}$ becomes larger, further decreasing $K_{\rm i}$. As shown in Fig. 8 and Fig. 9, this enables the proposed method to automatically adapt the grasping force according to the stiffness of the object, achieving appropriate deformation suppression without prior knowledge of object properties.

V. CONCLUSIONS

In this study, we proposed a novel parameter adaptation method based on object deformation that does not rely on learning. It enables high-speed processing and can be applied to objects with unknown mechanical and geometric properties. By combining an O-RLI-type and an O-ToF-type into a hybrid proximity sensor, the system quickly detects object deformation and appropriately reduces the grasping force before excessive force is applied. A key contribution of this work is the focus on the rate of change in the O-RLI-type output after contact, coupled with the extension of the MVDC (Multiple Virtual Dynamics-based Control) framework to serve as a planner for control parameters. This extension allows for smooth variation in the control parameters during grasping and avoids oscillatory behavior. Moreover, by integrating the approach with pre-grasp control, the method achieves delicate and unified grasping control across both the pre-contact and post-contact phases.

As future work, we will focus on adjusting the grasping force to prevent the object from being dropped. Additionally, we plan to cunduct experiments.

REFERENCES

[1] C. Blanes, M. Mellado, C. Ortiz, and Á. Valera, "Review. Technologies for robot grippers in pick and place operations for fresh fruits and vegetables," *Span. J. Agric. Res.*, vol. 9, pp. 1130–1141, Dec. 2011.

[2] Z. Wang, S. Hirai, and S. Kawamura, "Challenges and opportunities in robotic food handling: A review," *Front. Robot. AI*, vol. 8, 2022, Art. no. 789107.

[3] Y. Han et al., "Learning generalizable vision-tactile robotic grasping strategy for deformable objects via transformer," *IEEE/ASME Trans. Mechatron.*, vol. 30, no. 1, pp. 554-566, Feb. 2025.

[4] M. A. A. Ameur, A. M. El-Sayed, X. T. Yan, J. Mehnen, and A. M. Maier, "A novel opto-tactile sensing approach to enhance the handling of soft fruit," *Comput. Electron. Agric.*, vol. 235, Aug. 2025, Art. no. 110397.

[5] M. C. Welle, M. Lippi, H. Lu, J. Lundell, A. Gasparri, and D. Kragic, "Enabling robot manipulation of soft and rigid objects with vision-based tactile sensors," in *Proc. IEEE Int. Conf. Autom. Sci. Eng.*, 2023, pp. 1-7.

[6] W. Mandil, V. Rajendran, K. Nazari, and A. Ghalamzan-Esfahani, "Tactile-sensing technologies: Trends, challenges and outlook in agri-food manipulation," *Sensors*, vol. 23, no. 17, Aug. 2023, Art. no. 7362.

[7] S. Tokiwa, H. Arita, Y. Suzuki, and K. Tahara, "Integrated grasping controller leveraging optical proximity sensors for simultaneous contact, impact reduction, and force control," *IEEE Robot. Autom. Lett.*, vol. 9, no. 12, pp. 11633–11640, Dec. 2024.

[8] K. Koyama, Y. Suzuki, A. Ming, and M. Shimojo, "Grasping control based on time-to-contact method for a robot hand equipped with proximity sensors on fingertips," in *Proc. IEEE/RSJ Int. Conf. Intell. Robots Syst.*, 2015, pp. 504-510.

[9] Y. Suzuki, R. Yoshida, T. Tsuji, T. Nishimura, and T. Watanabe, "Grasping strategy for unknown objects based on real-time grasp-stability evaluation using proximity sensing," *IEEE Robot. Autom. Lett.*, vol. 7, no. 4, pp. 8643-8650, Oct. 2022.

[10] S. E. Navarro et al., "Proximity perception in human-centered robotics: A survey on sensing systems and applications," *IEEE Trans. Robot.*, vol. 38, no. 3, pp. 1599-1620, Jun. 2022.

[11] A. Yamaguchi and C. G. Atkeson, "Tactile behaviors with the vision-based tactile sensor FingerVision," *Int. J. Hum. Robot.*, vol. 16, no. 3, Jul. 2019, Art. no. 1940002.

[12] J. Di et al., "Using fiber optic bundles to miniaturize vision-based tactile sensors," *IEEE Trans. Robot.*, vol. 41, pp. 62-81, 2025.

[13] S. Wang, Y. She, B. Romero, and E. Adelson, "GelSight wedge: Measuring high-resolution 3D contact geometry with a compact robot finger," in *Proc. IEEE Int. Conf. Robot. Autom.*, 2021, pp. 6468-6475.

[14] H. Arita, H. Nakamura, T. Fujiki, and K. Tahara, "Smoothly connected preemptive impact reduction and contact impedance control," *IEEE Trans. Robot.*, vol. 39, no. 5, pp. 3536-3548, Oct. 2023.

[15] Y. Suzuki, T. Ito, and H. Sakai, "Development of modular-structured proximity sensor with hemispherical shape for end-effectors," in *Proc. Annu. Conf. SICE Syst. Integr. Div.*, 3E3-06, 2023.